IEEE Access
Multidisciplinary | Rapid Review | Open Access Journal

Received September 14, 2018, accepted October 8, 2018, date of publication December 10, 2018,
date of current version December 31, 2018.

Digital Object Identifier 10.1109/ACCESS.2018.2876883

Comparing Kalman Filters and Observers for Power System Dynamic State Estimation With Model Uncertainty and Malicious Cyber Attacks

JUNJIAN QI[1], (Senior Member, IEEE), AHMAD F. TAHA[2], (Member, IEEE), AND JIANHUI WANG[3], (Senior Member, IEEE)

[1]Department of Electrical and Computer Engineering, University of Central Florida, Orlando, FL 32816, USA
[2]Department of Electrical and Computer Engineering, The University of Texas at San Antonio, San Antonio, TX 78249, USA
[3]Department of Electrical Engineering, Southern Methodist University, Dallas, TX 75275, USA

Corresponding author: Junjian Qi (junjian.qi@ucf.edu)

ABSTRACT Kalman filters (KFs) and dynamic observers are two main classes of the dynamic state estimation (DSE) routines. The Power system DSE has been implemented by various KFs, such as the extended KF (EKF) and the unscented KF (UKF). In this paper, we discuss two challenges for an effective power system DSE: 1) model uncertainty and 2) potential cyber attacks and measurement faults. To address this, the cubature KF (CKF) and a nonlinear observer are introduced and implemented. Various KFs and the dynamic observer are then tested on the 16-machine 68-bus system given realistic scenarios under model uncertainty and different types of cyber attacks against synchrophasor measurements. It is shown that the CKF and the observer are more robust to model uncertainty and cyber attacks than their counterparts. Based on the tests, a thorough qualitative comparison is also performed for KF routines and observers.

INDEX TERMS Cyber attack, dynamic state estimation, Kalman filter, model uncertainty, non-Gaussian noise, observer, phasor measurement unit (PMU).

I. INTRODUCTION

State estimation is a crucial application in the energy management system (EMS). The well-known static state estimation (SSE) methods [1]–[5] assume that the power system is operating in quasi-steady state, based on which the static states—the voltage magnitude and phase angles of the buses—are estimated by using SCADA and/or synchrophasor measurements. SSE is critical for power system monitoring as it provides inputs for other EMS applications such as automatic generation control and optimal power flow.

However, SSE may not be sufficient for desirable situational awareness as the system states evolve more rapidly due to an increasing penetration of renewable generation and distributed energy resources. Therefore, dynamic state estimation (DSE) processes estimating the dynamic states (i.e., the internal states of generators) by using highly synchronized PMU measurements with high sampling rates will be critical for the wide-area monitoring, protection, and control of power systems.

For both SSE and DSE, two significant challenges make their practical application significantly difficult. First, the system model and parameters used for estimation can be inaccurate, which is often called *model uncertainty* [6], consequently deteriorating estimation in some scenarios. Second, the measurements used for estimation are vulnerable to cyber attacks, which in turn leads to compromised measurements that can greatly mislead the estimation.

For the first challenge, there are recent efforts on validating the dynamic model of the generator and calibrating its parameters [7], [8], which DSE can be based on. However, model validation itself can be very challenging. Hence, it is a more viable solution to improve the estimators by making them more robust to the model uncertainty.

For the second challenge, false data injection (FDI) attacks against SSE are proposed in [9]. After that it has been widely studied about how to mitigate this type of attack and further secure the monitoring and control of power grids [10]–[12]. In [13] an extended distributed state estimation is proposed for the tolerable FDI attacks on the SSE. In [14] an optimal PMU placement-based defense scheme is proposed for a least-effort data integrity attack on DC SSE. In [15] FDI attacks are designed to bypass the anomaly detection of the

Kalman filtering in DSE. Enhancement of Kalman filtering and temporal-based detection algorithm are proposed as countermeasures against the attacks. In [16] a risk mitigation strategy is proposed to eliminate the threat levels from the power grid's unknown inputs and potential cyber attacks based on a sliding-mode observer and an attack detection filter.

As for the approaches for performing DSE, there are mainly two classes of methods that have been proposed:

1) *Stochastic Estimators*: given a discrete-time representation of a dynamical system, the observed measurements, and the statistical information on process noise and measurement noise, Kalman filter (KF) and its many derivatives have been proposed that calculate the Kalman gain as a function of the relative certainty of the current state estimate and the measurements [17]–[21].
2) *Deterministic Observers*: given a continuous- or discrete-time dynamical system depicted by state-space matrices, a combination of matrix equalities and inequalities are solved, while guaranteeing asymptotic (or bounded) estimation error. The solution to these equations is often matrices that are used in an observer to estimate states and other dynamic quantities [22]–[24].

For power systems, DSE has been implemented by several stochastic estimators, such as extended Kalman filter (EKF) [25], [26], unscented Kalman filter (UKF) [27]–[31], square-root unscented Kalman filter (SR-UKF) [32]–[35], extended particle filter [36], [37], and ensemble Kalman filter [38]. While these techniques produce good estimation under nominal conditions, most of them lack the ability to deal with significant model uncertainty and malicious cyber attacks.

In order to improve the robustness of KFs, a generalized maximum-likelihood-type estimate is proposed in [39] and a two-stage KF is proposed in [40]. Besides, iterated EKF [41], H_∞ EKF [42], and robust UKF [43] are have also been developed for power system DSE.

The goal of this paper is to present alternatives that address these limitations. The paper contributions are summarized as follows. First, we use a nonlinear observer for the power system DSE problem that only requires computing a Luenberger-like gain matrix. This computation can be performed offline—and hence the presented observer is scalable for large-scale power networks. The observer requires obtaining scalar parameters that depict or bound the nonlinearities arising from the power system model. Numerical algorithms are provided to find these scalar parameters, in comparison with the observer design literature that obtains these scalars analytically which is impractical for large-scale power networks with high nonlinearities. The observer is endowed with the the following properties and virtues: (a) assumes that the generators' control inputs are not known to the state estimation method; (b) tolerates three classes of cyber-attacks (data integrity, denial of service, and replay attack) and other disturbances while accurately reconstructing the power system state within seconds of an attack or large disturbance; (c) assumes no statistical properties of the noise targeting process and measurement models; (d) requires no major real-time computation, in comparison with other estimation methods that are computationally expensive. To our knowledge, this contribution is the first of its kind in the power system DSE literature in comparison with Kalman filter derivatives.

Second, we introduce cubature Kalman filter (CKF) [21] that uses a more accurate cubature approach and possesses an important virtue of mathematical rigor rooted in the third-degree spherical-radial cubature rule for numerically computing Gaussian-weighted integrals. Without a stem at the center in the cubature-point set, CKF does not have the numerical instability problem of UKF [21], [34].

Last but not least, we design a realistic power system DSE problem by developing the system and measurement models and considering various practical scenarios such as unknown initial conditions, model uncertainties including process noise, unknown and unavailable inputs, and inaccurate parameters, and different types of measurement noises and cyber attacks against measurements. We present thorough numerical experiments to showcase the performance of the nonlinear observer and CKF in comparison with three other methods that have been recently applied to DSE. The comprehensive numerical tests are performed under a variety of conditions and disturbances, and the tests illustrate the potential of the presented estimation methods in correctly estimating the system's state. The conceptual strengths and limitations of different methods with significant model uncertainty and cyber attacks are also discussed.

The remainder of this paper is organized as follows. In Section II, we discuss the nonlinear dynamics of the multi-machine power system. The physical depictions of the model uncertainty and attack-threat model are introduced in Section III. The CKF and the nonlinear observer are introduced in Sections IV and V. Then, numerical results are given in Section VI. Finally, insightful remarks and conclusions are presented in Sections VII and VIII.

II. NONLINEAR MULTI-MACHINE POWER SYSTEM MODEL

Here we briefly discuss the power system model used for DSE. Each of the G generators is described by the fourth-order transient model in local d − q reference frame:

$$\begin{cases} \dot{\delta}_i = \omega_i - \omega_0 \\ \dot{\omega}_i = \dfrac{\omega_0}{2H_i}\Big(T_{\mathrm{m}i} - T_{\mathrm{e}i} - \dfrac{K_{\mathrm{D}i}}{\omega_0}(\omega_i - \omega_0)\Big) \\ \dot{e}'_{\mathrm{q}i} = \dfrac{1}{T'_{\mathrm{d}0i}}\Big(E_{\mathrm{fd}i} - e'_{\mathrm{q}i} - (x_{\mathrm{d}i} - x'_{\mathrm{d}i})i_{\mathrm{d}i}\Big) \\ \dot{e}'_{\mathrm{d}i} = \dfrac{1}{T'_{\mathrm{q}0i}}\Big(- e'_{\mathrm{d}i} + (x_{\mathrm{q}i} - x'_{\mathrm{q}i})i_{\mathrm{q}i}\Big), \end{cases} \tag{1}$$

where i is the generator serial number, δ_i is the rotor angle, ω_i is the rotor speed in rad/s, and $e'_{\mathrm{q}i}$ and $e'_{\mathrm{d}i}$ are the transient voltage along q and d axes; $i_{\mathrm{q}i}$ and $i_{\mathrm{d}i}$ are stator

currents at q and d axes; $T_{\mathrm{m}i}$ is the mechanical torque, $T_{\mathrm{e}i}$ is the electric air-gap torque, and $E_{\mathrm{fd}i}$ is the internal field voltage; ω_0 is the rated value of angular frequency, H_i is the inertia constant, and $K_{\mathrm{D}i}$ is the damping factor; $T'_{\mathrm{q0}i}$ and $T'_{\mathrm{d0}i}$ are the open-circuit time constants for q and d axes; $x_{\mathrm{q}i}$ and $x_{\mathrm{d}i}$ are the synchronous reactance and $x'_{\mathrm{q}i}$ and $x'_{\mathrm{d}i}$ are the transient reactance respectively at the q and d axes.

The $T_{\mathrm{m}i}$ and $E_{\mathrm{fd}i}$ in (1) are considered as inputs. The set of generators where PMUs are installed is denoted by $\mathcal{G}_{\mathrm{P}}$. For generator $i \in \mathcal{G}_{\mathrm{P}}$, the terminal voltage phaosr $E_{\mathrm{t}i} = e_{\mathrm{R}i} + je_{\mathrm{I}i}$ and current phasor $I_{\mathrm{t}i} = i_{\mathrm{R}i} + ji_{\mathrm{I}i}$ can be measured and are used as the outputs. Correspondingly, the state vector $\mathbf{x} \in \mathbb{R}^n$, input vector $\mathbf{u} \in \mathbb{R}^v$, and output vector $\mathbf{y} \in \mathbb{R}^p$ are

$$\mathbf{x} = \begin{bmatrix} \boldsymbol{\delta}^\top & \boldsymbol{\omega}^\top & \boldsymbol{e'_q}^\top & \boldsymbol{e'_d}^\top \end{bmatrix}^\top \tag{2a}$$

$$\mathbf{u} = \begin{bmatrix} \boldsymbol{T_m}^\top & \boldsymbol{E_{fd}}^\top \end{bmatrix}^\top \tag{2b}$$

$$\mathbf{y} = \begin{bmatrix} \boldsymbol{e_R}^\top & \boldsymbol{e_I}^\top & \boldsymbol{i_R}^\top & \boldsymbol{i_I}^\top \end{bmatrix}^\top. \tag{2c}$$

The $T_{\mathrm{e}i}$, $i_{\mathrm{d}i}$, and $i_{\mathrm{q}i}$ can be written as functions of $\boldsymbol{x}$:

$$\Psi_{\mathrm{R}i} = e'_{\mathrm{d}i}\sin\delta_i + e'_{\mathrm{q}i}\cos\delta_i \tag{3a}$$

$$\Psi_{\mathrm{I}i} = e'_{\mathrm{q}i}\sin\delta_i - e'_{\mathrm{d}i}\cos\delta_i \tag{3b}$$

$$I_{\mathrm{t}i} = \overline{\mathbf{Y}}_i(\boldsymbol{\Psi}_R + j\boldsymbol{\Psi}_I) \tag{3c}$$

$$i_{\mathrm{R}i} = \mathrm{Re}(I_{\mathrm{t}i}) \tag{3d}$$

$$i_{\mathrm{I}i} = \mathrm{Im}(I_{\mathrm{t}i}) \tag{3e}$$

$$i_{\mathrm{q}i} = \frac{S_{\mathrm{B}}}{S_{\mathrm{N}i}}(i_{\mathrm{I}i}\sin\delta_i + i_{\mathrm{R}i}\cos\delta_i) \tag{3f}$$

$$i_{\mathrm{d}i} = \frac{S_{\mathrm{B}}}{S_{\mathrm{N}i}}(i_{\mathrm{R}i}\sin\delta_i - i_{\mathrm{I}i}\cos\delta_i) \tag{3g}$$

$$e_{\mathrm{q}i} = e'_{\mathrm{q}i} - x'_{\mathrm{d}i}i_{\mathrm{d}i} \tag{3h}$$

$$e_{\mathrm{d}i} = e'_{\mathrm{d}i} + x'_{\mathrm{q}i}i_{\mathrm{q}i} \tag{3i}$$

$$T_{\mathrm{e}i} = \frac{S_{\mathrm{B}}}{S_{\mathrm{N}i}}(e_{\mathrm{q}i}i_{\mathrm{q}i} + e_{\mathrm{d}i}i_{\mathrm{d}i}), \tag{3j}$$

where $\Psi_i = \Psi_{\mathrm{R}i} + j\Psi_{\mathrm{I}i}$ is the voltage source, $\boldsymbol{\Psi}_R$ and $\boldsymbol{\Psi}_I$ are column vectors of all generators' $\Psi_{\mathrm{R}i}$ and $\Psi_{\mathrm{I}i}$, $e_{\mathrm{q}i}$ and $e_{\mathrm{d}i}$ are the terminal voltage at q and d axes, $\overline{\mathbf{Y}}_i$ is the ith row of the admittance matrix of the reduced network $\overline{\mathbf{Y}}$, and S_{B} and $S_{\mathrm{N}i}$ are the system base MVA and the base MVA for generator i, respectively.

In (3), the outputs $i_{\mathrm{R}i}$ and $i_{\mathrm{I}i}$ have been written as functions of $\mathbf{x}$. Similarly, the outputs $e_{\mathrm{R}i}$ and $e_{\mathrm{I}i}$ can also be written as function of $\mathbf{x}$:

$$e_{\mathrm{R}i} = e_{\mathrm{d}i}\sin\delta_i + e_{\mathrm{q}i}\cos\delta_i \tag{4a}$$

$$e_{Ii} = e_{\mathrm{q}i}\sin\delta_i - e_{\mathrm{d}i}\cos\delta_i. \tag{4b}$$

The dynamic model (1) can then be rewritten in a general state space form as

$$\begin{cases} \dot{\mathbf{x}} = \mathbf{A}\mathbf{x} + \mathbf{B}\mathbf{u} + \boldsymbol{\phi}(\mathbf{x}) \\ \mathbf{y} = \mathbf{h}(\mathbf{x}), \end{cases} \tag{5}$$

where

$$\mathbf{A} = \begin{bmatrix} \mathbf{I}_G & & \\ & \left(-\mathbf{K_D}\oslash 2\mathbf{H}\right)^{\mathrm{d}} & \\ & & \left(-\mathbf{1}_G \oslash \mathbf{T'_{d0}}\right)^{\mathrm{d}} \\ & & & \left(-\mathbf{1}_G \oslash \mathbf{T'_{q0}}\right)^{\mathrm{d}} \end{bmatrix},$$

$$\boldsymbol{B} = \begin{bmatrix} & & \\ \left(\omega_0\mathbf{1}_G \oslash 2\mathbf{H}\right)^{\mathrm{d}} & & \\ & \left(\mathbf{1}_G \oslash \mathbf{T'_{d0}}\right)^{\mathrm{d}} & \\ & & \end{bmatrix},$$

$$\boldsymbol{\phi} = \begin{bmatrix} -\omega_0\mathbf{1}_G \\ \left(\omega_0\mathbf{1}_G \oslash 2\boldsymbol{H}\right) \circledast \left(-\boldsymbol{T}_{\mathbf{e}} + \boldsymbol{K}_{\mathbf{D}}\mathbf{1}_G\right) \\ \left(\mathbf{1}_G \oslash \boldsymbol{T'_{d0}}\right) \circledast \left(-(\boldsymbol{x_d} - \boldsymbol{x'_d})\boldsymbol{i_d}\right) \\ \left(\mathbf{1}_G \oslash \boldsymbol{T'_{q0}}\right) \circledast \left((\boldsymbol{x_q} - \boldsymbol{x'_q})\boldsymbol{i_q}\right) \end{bmatrix},$$

and $\mathbf{h}$ include functions (3d)–(3e) and (4) for all generators, $\oslash$ and $\circledast$ are the Hadamard division/product (elementwise division/product) of a vector, and $(\mathbf{a})^{\mathrm{d}}$ gets a square diagonal matrix with the elements of vector $\mathbf{a}$ on the main diagonal.

Note that the model presented here is used for DSE for which the real-time inputs are assumed to be unavailable and $T_{\mathrm{m}i}$ and $E_{\mathrm{fd}i}$ only take steady-state values, mainly because these inputs are difficult to measure [26], [30]. However, when we simulate the power system to mimic the real system dynamics, we model an IEEE Type DC1 excitation system and a simplified turbine-governor system for each generator and thus $T_{\mathrm{m}i}$ and $E_{\mathrm{fd}i}$ change with time due to the governor and the excitation control, which leads to a tenth order generator model. More details about the model can be found in [16].

We do not directly use a detailed model including the exciter and governor as in [37] for the DSE mainly because 1) A good model should be simple enough to facilitate design [6], 2) it is harder to validate a detailed model and there are also more parameters that need to be calibrated [7], [8], [44], and 3) the computational burden can be higher for a more detailed model, which may not satisfy the requirement of real-time estimation.

III. MODEL UNCERTAINTY AND CYBER ATTACKS

The dynamic model of the power system can be written in a general state space form as

$$\begin{cases} \dot{\mathbf{x}} = \mathbf{f}(\mathbf{x}, \mathbf{u}) & \text{(6a)} \\ \mathbf{y} = \mathbf{h}(\mathbf{x}, \mathbf{u}), & \text{(6b)} \end{cases}$$

where $\mathbf{x} \in \mathbb{R}^n$, $\mathbf{u} \in \mathbb{R}^v$, and $\mathbf{y} \in \mathbb{R}^p$ are the vectors of the state, input, and output, and $\mathbf{f}$ and $\mathbf{h}$ are the nonlinear state transition functions and measurement functions. We rewrite (6) by separating the nonlinear term in the state transition functions as

$$\begin{cases} \dot{\mathbf{x}} = \mathbf{A}\mathbf{x} + \mathbf{B}\mathbf{u} + \boldsymbol{\phi}(\mathbf{x}) & (7a) \\ \mathbf{y} = \mathbf{h}(\mathbf{x}, \mathbf{u}), & (7b) \end{cases}$$

where $\boldsymbol{\phi}(\mathbf{x})$ represents the nonlinear term that models the interconnections in a multi-machine power system.

Two great challenges for an effective DSE are the model uncertainty and potential cyber attacks—discussed next.

A. MODEL UNCERTAINTY

The term *model uncertainty* refers to the differences or errors between models and reality. Various control and estimation theory studies investigated methods that addresses the discrepancy between the actual physics and models. The model uncertainty can be caused by the following reasons.

1) *Unknown inputs*: The unknown inputs against the system dynamics include $\mathbf{u}_\mathrm{d}$ (representing the unknown plant disturbances), $\mathbf{u}_\mathrm{u}$ (denoting the unknown control inputs), and $\mathbf{f}_\mathrm{a}$ (depicting potential generators actuator faults). For simplicity, we can combine them into one unknown input quantity $\mathbf{w} = \left[\mathbf{u}_\mathrm{d}^\top \ \mathbf{u}_\mathrm{u}^\top \ \mathbf{f}_\mathrm{a}^\top\right]^\top$. Defining $\mathbf{B}_\mathrm{w}$ to be the known weight distribution matrix of the distribution of unknown inputs with respect to each state-equation. The term $\mathbf{B}_\mathrm{w}\mathbf{w}$ models a general class of unknown inputs such as: nonlinearities, modeling uncertainties, noise, parameter variations, unmeasurable system inputs, model reduction errors, and actuator faults [45], [46]. For example, the equation $\dot{x}_1 = \dot{\delta}_1 = \omega_1 - \omega_0$ most likely has no unknown inputs, as there is no modeling uncertainty related to that process. Hence, the first row of $\mathbf{B}_\mathrm{w}$ can be identically zero. The process dynamics under unknown inputs can be written as follows:

$$\dot{\mathbf{x}} = \mathbf{A}\mathbf{x} + \mathbf{B}\mathbf{u} + \mathbf{B}_\mathrm{w}\mathbf{w} + \boldsymbol{\phi}(\mathbf{x}). \quad (8)$$

2) *Unavailable inputs*: Real-time inputs $\mathbf{u}$ can be unavailable, in which case the steady-states inputs $\mathbf{u}_0$ are used for estimation.
3) *Parameter inaccuracy*: The parameters in the system model can be inaccurate. For example, the reduced admittance matrix can be inaccurate when a fault or the following topology change are not detected.

B. CYBER ATTACKS

The National Electric Sector Cybersecurity Organization Resource (NESCOR) developed cyber-security failure scenarios with corresponding impact analyses [47]. The WAMPAC failure scenarios motivate the research in this paper include: a) *Measurement Data (from PMUs) Compromised due to PDC Authentication Compromise* and b) *Communications Compromised between PMUs and Control Center* [47]. Specifically, we consider the following three types of attacks [47], [48].

1) *Data integrity attacks*: An adversary attempts to corrupt the content of either the measurement or the control signals. A specific example of data integrity attacks are Man-in-the-Middle attacks, where the adversary intercepts the measurement signals and modifies them in transit. For DSE the PMU measurements can be modified and corrupted.
2) *Denial of Service (DoS) attack*: An attacker attempts to introduce a denial in communication of measurement. The communication of a sensor could be jammed by flooding the network with spurious packets. DoS attacks can happen at a variety of communication layers in a smart grid, such as the physical layer, Medium Access Control (MAC) layer, network and transport layer, and application layer. For DSE the consequence can be that the updated measurements cannot be sent to the control center.
3) *Replay attacks*: A special case of data integrity attacks, where the attacker replays a previous snapshot of a valid communication packet sequence that contains measurements in order to deceive the system. For DSE the PMU measurements can be changed to be those in the past.

For a data integrity cyber attack, it can be modeled by adding a vector $\mathbf{v}(t)$. Then the measurement model under cyber attacks becomes

$$\mathbf{y}(t) = \mathbf{h}\big(\mathbf{x}(t), \mathbf{u}(t)\big) + \mathbf{v}(t). \quad (9)$$

A DoS attack on output i at $t \in (t_1, t_2]$ can be modeled as

$$y_i = h_i\big(\mathbf{x}(t_1), \mathbf{u}(t_1)\big), \quad t \in (t_1, t_2]. \quad (10)$$

A replay attack on output i at $t \in [t_1, t_2]$ can be modeled as

$$y_i = h_i\big(\mathbf{x}(t - \Delta T), \mathbf{u}(t - \Delta T)\big), \quad t \in [t_1, t_2], \quad (11)$$

where $\Delta T = t_2 - t_1$.

In [49] the impact of false data injection attacks on dynamic state estimation is studied for linear dynamic systems, under Gaussian disturbances and attacks/biases and the effect of the false information is mathematically analyzed based on which corresponding defending strategies are investigated. In this paper, we consider cyber attacks against the PMU measurements used for DSE of nonlinear power systems. Specifically, we investigated the above-mentioned three types of attack models with no assumptions on the distribution of the noise.

Apart from cyber attacks against the PMU measurements, the commonly assumed Gaussian distribution of the PMU measurement noise may not hold for real data. Extensive results using field PMU data from WECC system has revealed that the Gaussian assumption is questionable [50]. Therefore, it would be valuable to evaluate the performance of different DSE methods under non-Gaussian noise.

IV. KALMAN FILTERS FOR POWER SYSTEM DSE

Unlike many estimation methods that are either computationally unmanageable or require special assumptions about the form of the process and observation models, KF only utilizes the first two moments of the state (mean and covariance) in its update rule [17]. It consists of two steps: in prediction step, the filter propagates the estimate from last time step to current time step; in update step, the filter updates the estimate using collected measurements. KF was initially developed for linear systems while for power system DSE the system equations and outputs have strong nonlinearity. Thus variants of KF that can deal with nonlinear systems have been introduced, such as EKF and UKF.

We consider a nonlinear system (without model uncertainty or attack vectors) in discrete-time form as

$$\begin{cases} \mathbf{x}_k = \mathbf{f}(\mathbf{x}_{k-1}, \mathbf{u}_{k-1}) + \mathbf{q}_{k-1} & \text{(12a)} \\ \mathbf{y}_k = \mathbf{h}(\mathbf{x}_k, \mathbf{u}_k) + \mathbf{r}_k, & \text{(12b)} \end{cases}$$

where $\mathbf{x}_k \in \mathbb{R}^n$, $\mathbf{u}_k \in \mathbb{R}^v$, and $\mathbf{y}_k \in \mathbb{R}^p$ are states, inputs, and observed measurements at time step k; the estimated mean and estimated covariance of the estimation error are $\mathbf{m}$ and $\mathbf{P}$; $\mathbf{f}$ and $\mathbf{h}$ are vectors consisting of nonlinear state transition functions and measurement functions; $\mathbf{q}_{k-1} \sim \mathcal{N}(0, \mathbf{Q}_{k-1})$ is the Gaussian process noise at time step $k-1$; $\mathbf{r}_k \sim \mathcal{N}(0, \mathbf{R}_k)$ is the Gaussian measurement noise at time step k; and $\mathbf{Q}_{k-1}$ and $\mathbf{R}_k$ are covariance matrices of $\mathbf{q}_{k-1}$ and $\mathbf{r}_k$.

A. EXTENDED KALMAN FILTER

Although EKF maintains the elegant and computationally efficient recursive update form of KF, it works well only in a 'mild' nonlinear environment, owing it to the first-order Taylor series approximation for nonlinear functions [21]. It is sub-optimal and can easily lead to divergence. Also, the linearization can be applied only if the Jacobian matrix exists and calculating Jacobian matrices can be difficult and error-prone. For DSE, EKF has been discussed in [25] and [26].

B. UNSCENTED KALMAN FILTER

The unscented transformation (UT) [51] is developed to address the deficiencies of linearization by providing a more direct and explicit mechanism for transforming mean and covariance information. Based on UT, Julier and Uhlmann [19], [20] propose the UKF as a derivative-free alternative to EKF. The Gaussian distribution is represented by a set of deterministically chosen sample points called sigma points. The UKF has been applied to power system DSE, for which no linearization or calculation of Jacobian matrices is needed [27]–[31].

In UKF, a total of $2n+1$ sigma points (denoted by $\boldsymbol{\mathcal{X}}$) are calculated from the columns of the matrix $\eta\sqrt{\mathbf{P}}$ as

$$\begin{cases} \boldsymbol{\mathcal{X}}^{(0)} = \mathbf{m} & \text{(13a)} \\ \boldsymbol{\mathcal{X}}^{(i)} = \mathbf{m} + \left[\eta\sqrt{\mathbf{P}}\right]_i, \quad i = 1, \ldots, n & \text{(13b)} \\ \boldsymbol{\mathcal{X}}^{(i)} = \mathbf{m} - \left[\eta\sqrt{\mathbf{P}}\right]_i, \quad i = n+1, \ldots, 2n & \text{(13c)} \end{cases}$$

with weights

$$\begin{cases} \boldsymbol{w}_m^{(0)} = \dfrac{\lambda}{n+\lambda} & \text{(14a)} \\ \boldsymbol{w}_c^{(0)} = \dfrac{\lambda}{n+\lambda} + (1 - \alpha^2 + \beta) & \text{(14b)} \\ \boldsymbol{w}_m^{(i)} = \dfrac{1}{2(n+\lambda)}, \quad i = 1, \ldots, 2n & \text{(14c)} \\ \boldsymbol{w}_c^{(i)} = \dfrac{1}{2(n+\lambda)}, \quad i = 1, \ldots, 2n, & \text{(14d)} \end{cases}$$

where the matrix square root of a positive semidefinite matrix $\mathbf{P}$ is a matrix $\mathbf{S} = \sqrt{\mathbf{P}}$ such that $\mathbf{P} = \mathbf{S}\mathbf{S}^\top$, $\boldsymbol{w}_m$ and $\boldsymbol{w}_c$ are respectively weights for the mean and the covariance, $\eta = \sqrt{n+\lambda}$, λ is a scaling parameter defined as $\lambda = \alpha^2(n+\kappa) - n$, and α, β, and κ are constants and α and β are nonnegative.

The basic idea of UKF is to choose the sigma-point set to capture a number of low-order moments of the prior density of the states as correctly as possible, and then compute the posterior statistics of the nonlinear functions (either state transition functions $\mathbf{f}$ or measurement functions $\mathbf{h}$) by UT which approximates the mean and the covariance of the nonlinear function by a weighted sum of projected sigma points.

However, for the sigma-points, the stem at the center (the mean) is highly significant as it carries more weight which is usually negative for high-dimensional systems. Therefore, the UKF is supposed to encounter numerical instability troubles when used in high-dimensional problems. Several techniques including the square-root unscented Kalman filter (SR-UKF) have been proposed to solve this problem [32], [33]. Recently SR-UKF has been applied to DSE in power systems in [34].

C. CUBATURE KALMAN FILTER

EKF and UKF can suffer from the curse of dimensionality while becoming detrimental in high-dimensional state-space models of size twenty or more—especially when there are high degree of nonlinearities in the equations that describe the state-space model [21], [52], which is exactly the case for power systems. Making use of the spherical-radial cubature rule, Arasaratnam and Haykin [21] propose CKF, which possesses an important virtue of mathematical rigor rooted in the third-degree spherical-radial cubature rule for numerically computing Gaussian-weighted integrals. In this paper we will apply CKF to power system DSE. Compared with EKF, UKF, and SR-UKF, CKF has the following advantages:

1) Compared with EKF and similar to UKF and SR-UKF, CKF is also derivative-free and is easier for application.
2) Similar to UKF and SR-UKF, CKF also uses a weighted set of symmetric points to approximate the

Gaussian distribution. But the cubature-point set does not have a stem at the center and thus does not have the numerical instability problem of UKF discussed in Section IV-B.

3) UKF treats the derivation of the sigma-point set for the prior density and the computation fo posterior statistics as two disjoint problems. By contrast, CKF directly derives the cubature-point set to accurately compute the first two-order moments of a nonlinear transformation, therefore naturally increasing the accuracy of the numerical estimates for moment integrals [21].
4) As suboptimal Bayesian filters, EKF, UKF, and CKF all have some robustness to model uncertainties and measurement outliers [53]. The extent of robustness depends on their ability to accurately deal with the nonlinear transformations. The EKF is the least robust method due to a first-order Taylor series approximation of the nonlinear functions while the CKF has the highest robustness thanks to its more accurate cubature approach, which will be validated in the result section.

V. NONLINEAR OBSERVERS FOR POWER SYSTEM DSE

Dynamic observers have been thoroughly investigated for different classes of systems. To mention a few, they have been developed for linear time-invariant (LTI) systems, nonlinear time-invariant (NLTI) systems, LTI and NLTI systems with unknown inputs, sensor and actuator faults, stochastic dynamical systems, and hybrid systems [22], [23].

Most observers utilize the plant's outputs and inputs to generate real-time estimates of the plant states, unknown inputs, and sensor faults. The cornerstone is the innovation function—sometimes a simple gain matrix designed to nullify the effect of unknown inputs and faults. Linear and nonlinear functional observers, sliding-mode observers, unknown input observers, and observers for fault detection and isolation are all examples on developed observers for different classes of systems, under different assumptions [24].

In comparison with KF techniques, nonlinear and robust observers have not been utilized for power system DSE. However, they inherently possess the theoretical, technical, and computational capabilities to perform good estimation of the power system's dynamic states. As for implementation, observers are simpler than KFs. For observers, matrix gains are computed offline to guarantee the asymptotic stability of the estimation error or the boundedness of the estimation error within a neighborhood of the origin.

Here, we present a recently developed observer in [54] that can be applied for DSE in power systems. This observer assumes that the nonlinear function $\boldsymbol{\phi}(\mathbf{x})$ in (7) satisfies the one-sided Lipschitz condition. Specifically, there exists $\rho \in \mathbb{R}$ such that $\forall\, \mathbf{x}_1, \mathbf{x}_2$ in a region D including the origin with respect to the state $\mathbf{x}$, there is

$$\langle \boldsymbol{\phi}(\mathbf{x}_1) - \boldsymbol{\phi}(\mathbf{x}_2), \mathbf{x}_1 - \mathbf{x}_2 \rangle \leq \rho \, \|\mathbf{x}_1 - \mathbf{x}_2\|^2,$$

Algorithm 1 Obtaining One-Sided Lipschitz Constant ρ

input $\boldsymbol{\phi}(\mathbf{x})$ and $\mathcal{D}$
$\rho_0 \leftarrow -\infty$
for $i = 1 : n_{\mathcal{D}}$ **do**
  $\mathbf{x} \leftarrow \mathbf{x}_i$
  compute $\rho_i = \left[\lambda_{\max}\left(\frac{1}{2}\left(\frac{\partial \boldsymbol{\phi}(\mathbf{x})}{\partial \mathbf{x}} + \left(\frac{\partial \boldsymbol{\phi}(\mathbf{x})}{\partial \mathbf{x}}\right)^{\top}\right)\right)\right]$
  $\rho_i = \max(\rho_{i-1}, \rho_i)$
end for
output $\rho \leftarrow \rho_{n_{\mathcal{D}}}$

where $\langle \cdot, \cdot \rangle$ is the inner product. Besides, the nonlinear function is also assumed to be quadratically inner-bounded as

$$\left(\boldsymbol{\phi}(\mathbf{x}_1) - \boldsymbol{\phi}(\mathbf{x}_2)\right)^{\top}\left(\boldsymbol{\phi}(\mathbf{x}_1) - \boldsymbol{\phi}(\mathbf{x}_2)\right) \leq \mu \, \|\mathbf{x}_1 - \mathbf{x}_2\|^2 + \varphi \, \langle \boldsymbol{\phi}(\mathbf{x}_1) - \boldsymbol{\phi}(\mathbf{x}_2), \mathbf{x}_1 - \mathbf{x}_2 \rangle,$$

where μ and φ are real numbers. Similar results related to the dynamics of multi-machine power systems established a similar quadratic bound on the nonlinear component (see [55]). To determine the constants ρ, μ, and φ, a simple offline algorithm can be implemented. For example, we can define a *region of interest* $\mathcal{D} \subset \mathbb{R}^n$ to be the state-space region where the system operates. For the multi-machine power network, this region is the intersection of all upper and lower bounds of states, which can be written as

$$\mathcal{D} = [\mathbf{x}_1^{\min}, \mathbf{x}_1^{\max}] \times [\mathbf{x}_2^{\min}, \mathbf{x}_2^{\max}] \times \cdots \times [\mathbf{x}_n^{\min}, \mathbf{x}_n^{\max}].$$

This region $\mathcal{D}$ can be obtained by the method discussed in [56]. We sample random points in this region. Denser sampling yields a more realistic Lipschitz constant, while requiring more computational time. Let $n_{\mathcal{D}}$ be the total number of samples inside $\mathcal{D}$. Algorithm 1 includes the steps required to obtain ρ. Specifically, ρ can be calculated from

$$\rho = \limsup\left(\beta\left(\frac{\partial \boldsymbol{\phi}}{\partial \mathbf{x}}\right)\right)$$

for all $\mathbf{x} \in \mathcal{D}$, where $\beta(\mathbf{H})$ denotes the logarithmic matrix norm of matrix $\mathbf{H}$ defined as

$$\beta(\mathbf{H}) = \lim_{\epsilon \to 0} \frac{\|\mathbf{I} + \epsilon \mathbf{H}\| - 1}{\epsilon},$$

where $\|\cdot\|$ represents any matrix norm. It is shown in [57] that the logarithmic matrix norm can also be written as

$$\beta(\mathbf{H}) = \lambda_{\max}\left(\frac{1}{2}\left(\mathbf{H} + \mathbf{H}^{\top}\right)\right) \leq \|\mathbf{H}\|.$$

At each iteration, we obtain the maximum eigenvalue of $\frac{1}{2}\left(\frac{\partial \boldsymbol{\phi}(\mathbf{x})}{\partial \mathbf{x}} + \left(\frac{\partial \boldsymbol{\phi}(\mathbf{x})}{\partial \mathbf{x}}\right)^{\top}\right)$ where the Jacobian of the nonlinear function is evaluated at the ith sampled point. Finally, ρ is computed by finding the maximum value of $\beta(\cdot)$ over $\mathcal{D}$.

Algorithm 1 is an offline search method to obtain the one-side Lipschitz constant. The most computationally intensive step of Algorithm 1 is finding the eigenvalues of an n-by-n matrix (where n is the state dimension, i.e., $\boldsymbol{x} \in \mathbb{R}^n$),

followed by finding the maximum eigenvalue. There are many algorithms to find the eigenvalues of a matrix, but the majority rely on matrix decompositions. Classical algorithms replying on the singular value decomposition (SVD) require $\mathcal{O}(n^3)$, and since the algorithm is repeated $n_{\mathcal{D}}$ times, then the computational complexity of Algorithm 1 is $\mathcal{O}(n^3 \cdot n_{\mathcal{D}})$.

To compute the quadratic inner-boundedness constants μ and φ, a similar algorithm can be obtained. In particular, instead of sampling over individual $\mathbf{x}_i \in \mathcal{D}$, two state-space samples $\mathbf{x}_i$ and $\mathbf{x}_j$ can be sampled at each iteration (i, j), and

$$\big(\boldsymbol{\phi}(\mathbf{x}_i) - \boldsymbol{\phi}(\mathbf{x}_j)\big)^\top \big(\boldsymbol{\phi}(\mathbf{x}_i) - \boldsymbol{\phi}(\mathbf{x}_j)\big) \leq \mu_{i,j} \|\mathbf{x}_i - \mathbf{x}_j\|^2 + \varphi_{i,j} \langle \boldsymbol{\phi}(\mathbf{x}_i) - \boldsymbol{\phi}(\mathbf{x}_j), \mathbf{x}_i - \mathbf{x}_j \rangle,$$

is evaluated iteratively for all possible permutations $\mathbf{x}_i$ and $\mathbf{x}_j$ in $\mathcal{D}$ to obtain the maximum values for μ and φ that satisfy the above inequality. Following these assumptions, the dynamics of this observer can be written as

$$\dot{\hat{\mathbf{x}}}. = \mathbf{A}\dot{\hat{\mathbf{x}}} + \mathbf{B}\mathbf{u} + \boldsymbol{\phi}(\dot{\hat{\mathbf{x}}}) + \mathbf{L}\big(\mathbf{y} - \mathbf{C}\dot{\hat{\mathbf{x}}}\big), \tag{15}$$

where $\mathbf{L}$ is a matrix gain determined by Algorithm 2. First, given the Lipschitz constants ρ, φ, and μ, the linear matrix inequality in (16) is solved for positive constants ϵ_1, ϵ_2, and σ and a symmetric positive semi-definite matrix $\mathbf{P}$. Utilizing the solution $\mathbf{L}$ in (17), the state estimates generated from (15) are guaranteed to converge to the actual values of the states.

Algorithm 2 Observer Design Algorithm

compute constants ρ, μ, and φ via an offline search algorithm

solve this LMI for $\epsilon_1, \epsilon_2, \sigma > 0$ and $\mathbf{P} = \mathbf{P}^\top \succ O$:

$$\begin{bmatrix} \mathbf{A}^\top\mathbf{P} + \mathbf{P}\mathbf{A} + (\epsilon_1\rho + \epsilon_2\mu)\mathbf{I}_n & \\ -\sigma\,\mathbf{C}^\top\mathbf{C} & \mathbf{P} + \dfrac{\varphi\,\epsilon_2 - \epsilon_1}{2}\mathbf{I}_n \\ \hline \left(\mathbf{P} + \dfrac{\varphi\,\epsilon_2 - \epsilon_1}{2}\mathbf{I}_n\right)^\top & -\epsilon_2\mathbf{I}_n \end{bmatrix} < 0. \tag{16}$$

obtain the observer design gain matrix $\mathbf{L}$:

$$\mathbf{L} = \frac{\sigma}{2}\mathbf{P}^{-1}\mathbf{C}^\top. \tag{17}$$

simulate the observer design given in (15)

Note that the observer design utilizes linearized measurement functions $\mathbf{C}$, which for power system DSE can be obtained by linearizing the nonlinear functions in (7). However, since the measurement functions have high nonlinearity, when performing the estimation we do not use (15), as in [54], but choose to directly use the nonlinear measurement functions as

$$\dot{\hat{\mathbf{x}}}. = \mathbf{A}\dot{\hat{\mathbf{x}}} + \mathbf{B}\mathbf{u} + \boldsymbol{\phi}(\dot{\hat{\mathbf{x}}}) + \mathbf{L}\big(\mathbf{y} - \mathbf{h}(\dot{\hat{\mathbf{x}}})\big). \tag{18}$$

The main principle behind the observer design is to minimize the difference between the estimated measurements (i.e., $\dot{\hat{\mathbf{y}}}(t)$) and the actual ones ($\mathbf{y}(t)$) through the innovation term $\mathbf{L}\big(\mathbf{y} - \mathbf{h}(\dot{\hat{\mathbf{x}}})\big)$. The objective of this term is to nullify/minimize the discrepancies due to errors in the estimation, model uncertainties, measurement noise, or attack vectors. The difference between $\mathbf{y}(t)$ and $\dot{\hat{\mathbf{y}}}(t)$ yields an estimate for the attack vector. Hence, the states evolution for the observer are indirectly aware of the differences between measured and potentially corrupt outputs and the estimated ones. Given the solution to the linear matrix inequality (LMI), the estimation error dynamics will be asymptotically stable. Finally, it is important to mention that Algorithm 2 can be performed offline, which implies that the observer in real-time only requires a state-estimate update while all other quantities are given; after finding $\mathbf{L}$ one can simulate (18) without needing to perform other computations.

For Algorithm 2, we solve the LMI (16). Primal-dual interior-point methods for LMIs/SDPs have a worst-case complexity estimate of $\mathcal{O}\left(m^{2.75}L^{1.5}\right)$, where m is the number of variables (a function of n and n_y, the state and output dimensions) and L is the number of constraints [58]. In various problems arising in estimation/control, it is shown that the complexity estimate is closer to $\mathcal{O}\left(m^{2.1}L^{1.2}\right)$; see [58] and references therein. With that in mind, recent advancements in semidefinite programming that utilize the sparse nature of the state-space matrices can be exploited to improve the computational efficiency.

VI. NUMERICAL RESULTS

Here we test EKF, UKF, SR-UKF, CKF, and the nonlinear observer on the 16-machine 68-bus system extracted from Power System Toolbox (PST) [59]. The one-line diagram of the test system is shown in Fig. 1. For the DSE we consider both unknown inputs to the system dynamics and cyber attacks against the measurements including data integrity, DoS, and replay attacks; see Section III. All tests are performed on a 3.2-GHz Intel(R) Core(TM) i7-4790S desktop.

For simulating the power system to mimic the real system dynamics, we model an IEEE Type DC1 excitation system and a simplified turbine-governor system, which leads to a 10th order generator model. More details about the model can be found in [16]. The simulation data is generated as follows.

1) The simulation data is generated by the detailed 10-th order model. The sampling rate is 60 samples/s.
2) In order to generate dynamic response, a three-phase fault is applied at bus 6 of branch $6-11$ and is cleared at the near and remote ends after 0.05 and 0.1 s.
3) All generators are equipped with PMUs at their terminal buses. The real and imaginary parts of the voltage phasor and current phasor are considered as measurements.
4) The sampling rate of the measurements is set to be 60 frames/s to mimic the PMU sampling rate.
5) Gaussian process noise is added and the corresponding process noice covariance is a diagonal matrix, whose

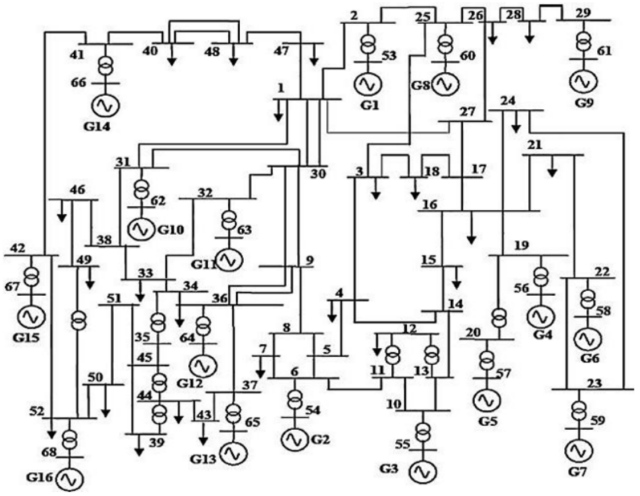

FIGURE 1. 16-machine 68-bus system.

diagonal entries are the square of 5% of the largest state changes [36].

6) Gaussian noise with variance 0.01^2 is added to the PMU measurements.
7) Each entry of the unknown input coefficients $\mathbf{B}_w$ is a random number that follows normal distribution with zero mean and variance as the square of 50% of the largest state changes. Note that the variance here is much bigger than that of the process noise.
8) The unknown input vector $\mathbf{w}$ is set as a function of t as

$$\mathbf{w}(t) = \begin{bmatrix} 0.5\cos(\omega_u t) \\ 0.5\sin(\omega_u t) \\ 0.5\cos(\omega_u t) \\ 0.5\sin(\omega_u t) \\ -e^{-5t} \\ 0.2\,e^{-t}\cos(\omega_u t) \\ 0.2\cos(\omega_u t) \\ 0.1\sin(\omega_u t) \end{bmatrix},$$

where $\omega_u = 100$ is the frequency of the given signals. The unknown inputs are manually chosen, showing different scenarios for inaccurate model and parameters without a predetermined distribution.

For DSE we use the fourth-order generator model in [33] and [34]. The Kalman filters and the observer are set as follows.

1) DSE is performed on the post-contingency system on time period [0, 10 s], which starts from the fault clearing.
2) The initial estimated mean of the rotor speed is set to be ω_0 and that for the other states is set to be twice of the real initial states.
3) The initial estimation error covariance is set to be $0.1\mathbf{I}_n$.
4) As mentioned before, the covariance of the process noise is set as a diagonal matrix, whose diagonal entries are the square of 5% of the largest state changes [36].

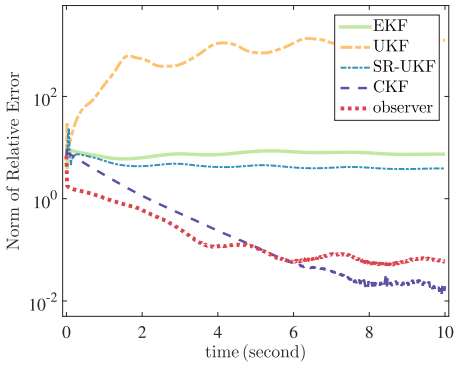

FIGURE 2. Norm of relative error of the states in Scenario 1.

5) The covariance for the measurement noise is a diagonal matrix, whose diagonal entries are 0.01^2, as in [36].
6) For both UKF and SR-UKF, $2n + 1$ sigma points are used in the unscented transformation.
7) For UKF and SR-UKF, a popular heuristic $n + \kappa = 3$ proposed in [60] is used to choose the parameter κ in unscented transformation in order to minimize the moments of the standard Gaussian and the sigma points up to the fourth order.
8) For UKF is performed by using the EKF/UKF toolbox [61], in which the function 'schol' is used to calculate the lower triangular Cholesky factor of a matrix and can get an output even when the matrix is not positive semidefinite [34].
9) For the observer in Section V, the LMI (16) is solved via CVX on MATLAB [62]. The Lipschitz constants in Algorithm 2 are set as $\rho = 10, \mu = 1$, and $\varphi = 1$.
10) The mechanical torque and internal field voltage are considered as unavailable inputs and take steady-state values, because they are difficult to measure [26], [30].
11) On [0, 1 s] the reduced admittance matrix is the one for the pre-contingency state.
12) Data integrity, DoS, and replay attacks, as discussed in Section III-B, are added to the PMU measurements.

A. SCENARIO 1: DATA INTEGRITY ATTACK

Data integrity attack is added to the first eight measurements, i.e., the real parts of the voltage phasors. The compromised measurements are obtained by scaling the real measurements by 0.6 and 1/0.6, respectively, for the first four and the last four measurements. The 2-norm of the relative error of the states, $||(\mathbf{x}(t) - \hat{\mathbf{x}}(t))/\mathbf{x}(t)||_2$, for different estimation methods is shown in Fig. 2. It is seen that the error norm for both CKF and the observer can quickly converge among which the observer converges faster, while the value that CKF converges to is slightly smaller in magnitude. By contrast, EKF, UKF, and SR-UKF do not perform as well.

We also show the states estimation for Generator 1 in Fig. 3. It is seen that the observer and CKF converge rapidly

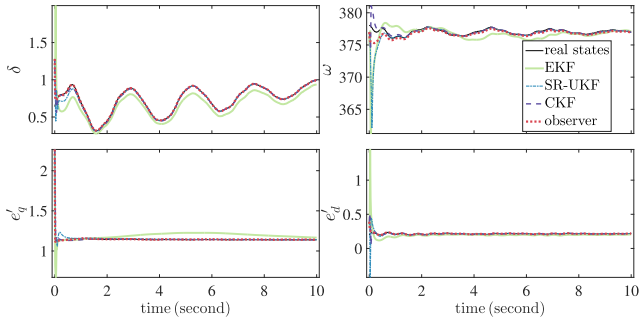

FIGURE 3. Estimated states by EKF, SR-UKF, CKF, and observer in Scenario 1.

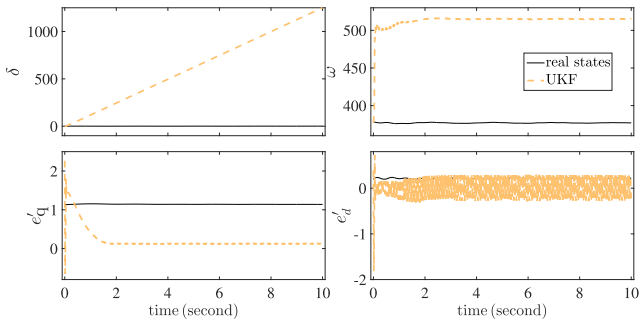

FIGURE 4. Estimated states by UKF in Scenario 1.

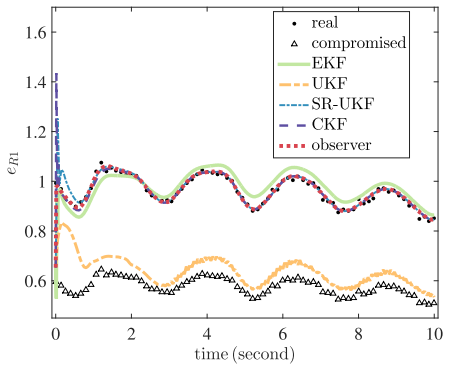

FIGURE 5. Estimated values for the first measurement in Scenario 1.

while the EKF fails to converge after 10 seconds. The estimation for UKF is separately shown in Fig. 4 because its estimated states are far away from the real states. Note that the real system dynamics are stable while the UKF estimation misled by the data integrity attack indicates that the system is unstable.

The real, compromised, and estimated values for the first measurement are shown in Fig. 5. For the observer, CKF, and SR-UKF, the estimated measurements are very close to the actual ones. For EKF there are some differences between the estimates and the real values, while UKF's generated estimates are close to the compromised measurements, indicating that it is completely misled by the cyber attack.

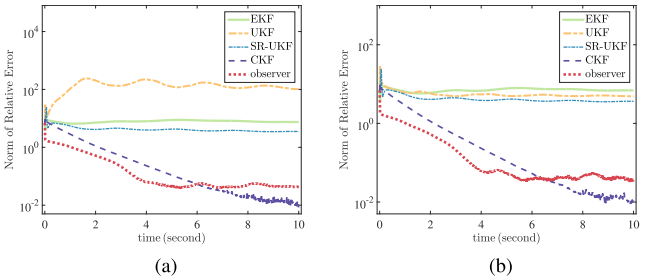

FIGURE 6. Norm of relative error of the states. (a) Scenario 2. (b) Scenario 3.

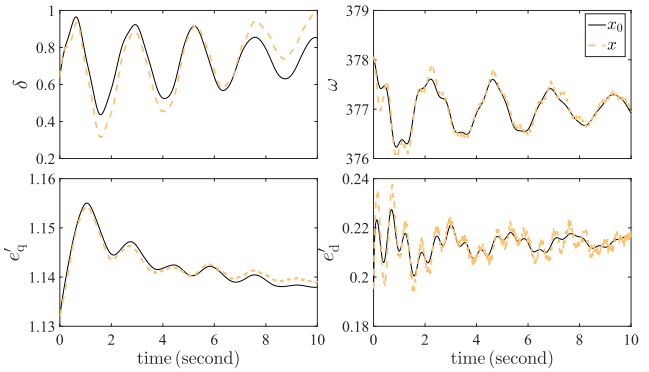

FIGURE 7. System states with and without model uncertainty in Scenario 1.

B. SCENARIO 2: DOS ATTACK AND SCENARIO 3: REPLAY ATTACK

The first eight measurements are kept unchanged for $t \in [3\,\text{s},\ 6\,\text{s}]$ to mimic the DoS attack in which case the updated measurements cannot be sent to the control center due to, for example, jammed communication between PMU to PDC or between PDC to the control center [47].

Replay attack is added on the first eight measurements for which there is $y_i(t) = y_i(t-3)$ for $t \in [3\,\text{s},\ 6\,\text{s}]$.

The 2-norm of the relative error of the states is shown in Fig. 6 and the results are very similar to those in Scenario 1.

C. DISCUSSION ON MODEL UNCERTAINTY ESTIMATION

We take Scenario 1 as an example to discuss the performance of different methods in dealing with model uncertainty. The states of the system with and without model uncertainty, including unknown inputs, unavailable inputs, and parameter inaccuracy, are separately denoted by $\mathbf{x}$ and $\mathbf{x}_0$, which are shown in Fig. 7. The difference between $\mathbf{x}$ and $\mathbf{x}_0$, $\mathbf{x} - \mathbf{x}_0$, is shown in Fig. 8. The estimated model uncertainty for Generator 1 by EKF, SR-UKF, CKF, and the observer is shown in Fig. 9 and that for UKF is shown in Fig. 10. It is seen that SR-UKF, CKF, and the observer can estimate the model uncertainty pretty well while the EKF does not perform as well and the UKF has the worst performance for which the model uncertainty estimation is largely misled by the data integrity attack.

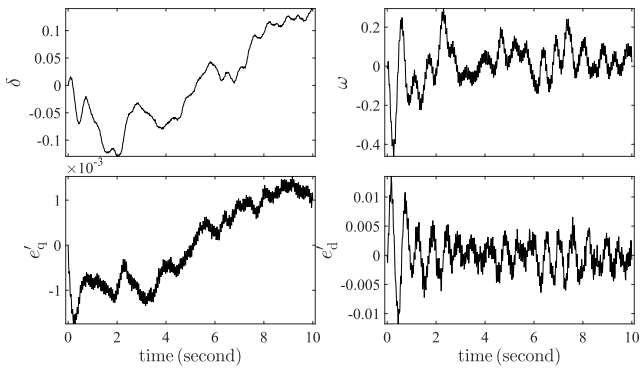

FIGURE 8. The $x - x_0$ in Scenario 1.

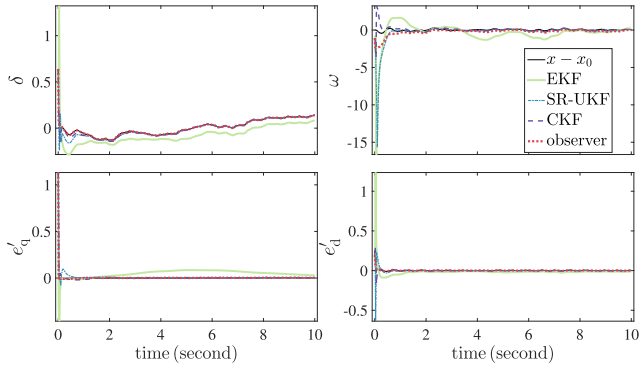

FIGURE 9. Estimated model uncertainty for EKF, SR-UKF, CKF, and the observer in Scenario 1.

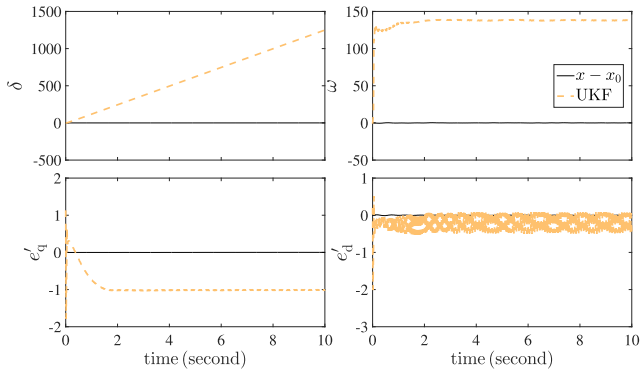

FIGURE 10. Estimated model uncertainty for UKF in Scenario 1.

D. DISCUSSION ON CYBER ATTACK DETECTION

The normalized innovation ratio of the jth measurement at time step k is defined as the ratio between the deviation of its actual measurement from the predicted measurement and the expected standard deviation [27], [29], [30]:

$$\lambda_{k,j} = \frac{y_{k,j} - \hat{y}_{k|k-1,j}}{\sqrt{\mathbf{P}_{yy,k|k-1,j}}}, \tag{19}$$

where $\mathbf{P}_{yy,k|k-1,j}$ is the jth diagonal element of the measurement covariance.

The normalized innovation ratio for all of the measurements for EKF, UKF, SR-UKF, and CKF in Scenario 1 are

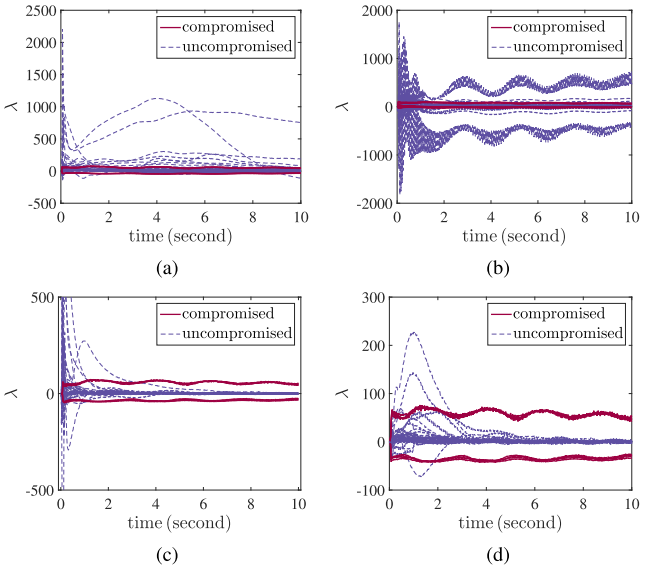

FIGURE 11. Cyber attack detection in Scenario 1 for (a) EKF, (b) UKF, (c) SR-UKF, and (d) CKF.

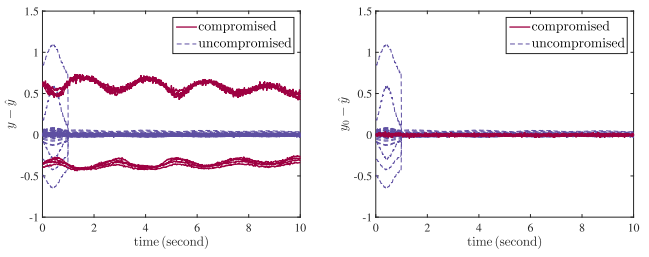

FIGURE 12. Norm of relateive error of the states. (a) attack detection and real and estimated measurements for the observer in Scenario 1.

shown in Fig. 11. It is seen that for EKF and UKF the normalized innovation ratios of a few uncompromised measurements are greater than those for the compromised measurements, which means that EKF and UKF cannot correctly detect the compromised measurements. For SR-UKF and CKF, after a few seconds (in the first second some uncompromised measurements can have bigger normalized innovation ratios mainly because the parameters used for estimation in that time period are inaccurate), the normalized innovation ratios for compromised measurements are significantly greater than those for the uncompromised ones, and the compromised measurements can be detected by a properly chosen threshold. Compared to SR-UKF, CKF has a better performance. For Scenarios 2–3 the results are similar and are not presented.

For the observer, since there is no measurement covariance we will detect cyber attacks against the measurements directly using the measurement innovation $y_{k,j} - \hat{y}_{k|k-1,j}$, which is shown in Fig. 12a for Scenario 1. It is seen that after the first second in which the parameters are inaccurate the measurement innovation of the compromised measurements are significantly greater than those of the uncompromised

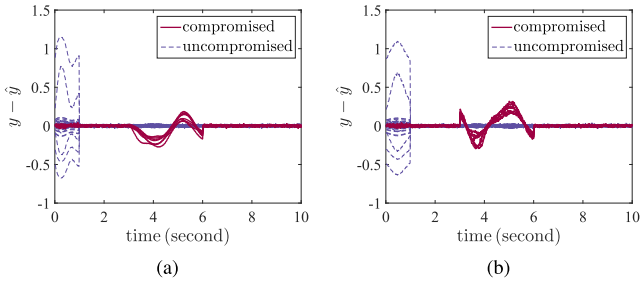

FIGURE 13. Cyber attack detection in Scenario 2 and Scenario 3 for the observer.

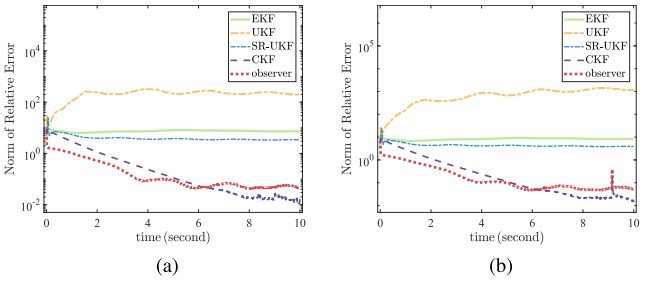

FIGURE 14. Norm of relative error of the states under different measurement noises. (a) Laplace noise and (b) Cauchy noise.

ones and thus the compromised measurements can be easily detected. In Fig. 12b we also show the different between the real and estimated measurements, $y_0 - \hat{y}$. For both the compromised and uncompromised measurements, the estimated measurements from the observer can almost immediately converge to the real measurements after the first second.

In Fig. 13 we show the measurement innovation of the observer for Scenario 2 (Fig. 13a) and Scenario 3 (Fig. 13b), which indicates that the compromised measurements can also be detected by the observer.

E. NON-GAUSSIAN MEASUREMENT NOISE

We performed DSE under data integrity attack in Scenario 1 with non-Gaussian measurement noise, including the Laplace noise and Cauchy noise. Laplace noise with mean m and scale s is generated by

$$r_{\text{Laplace}} = m - s\,\text{sgn}(U_1)\ln(1 - 2|U_1|), \tag{20}$$

where m is set to be zero, s is chosen as 0.02, and U_1 is a random number sampled from a uniform distribution in the interval $(-0.5, 0.5]$. Cauchy noise is obtained by sampling the inverse cumulative distribution function of the distribution

$$r_{\text{Cauchy}} = a + b\tan\big(\pi(U_2 - 0.5)\big), \tag{21}$$

where $a = 0$ and $b = 10^{-4}$ are the location and scale parameters, and U_2 is randomly sampled from the uniform distribution on the interval $(0, 1)$.

The norms of the relative error of the states under Laplace and Cauchy noises are shown in Fig. 14. Similar to the case with Gaussian noise, the observer and CKF also outperform the other methods. Under Laplace noise, the performance of different methods are similar to that under Gaussian noise. However, under Cauchy noise that has a super-heavy tailed distribution with no defined moments, the performance of all methods degrade, converging to a much bigger norm of relative error of the states.

F. COMPUTATIONAL EFFICIENCY

For the above three scenarios, the time for estimation by different methods is listed in Table 1. It is seen that EKF and the observer are more efficient than the other methods while CKF is the least efficient. Note that the time reported here is from MATLAB implementations. It can be greatly reduced by more efficient, such as C-based implementations.

TABLE 1. Time for performing estimation for 10 seconds.

EKF	UKF	SR-UKF	CKF	observer
4.0 s	11.2 s	11.6 s	9.9 s	5.8 s

VII. COMPARING KALMAN FILTERS AND OBSERVERS

Here, various functionalities of DSE methods and their strengths and weaknesses relative to each functionality are presented based on (a) the technical, theoretical capabilities and (b) experimental results in Section VI.

- *Nonlinearities in Dynamics:* UKF, SR-UKF, CKF, and the observer in Section V all work on nonlinear systems while EKF assumes linearized system dynamics. Besides, the presented observer uses linearized measurement functions for design but directly uses nonlinear measurement functions for estimation.
- *Solution Feasibility:* The main principle that governs the design of most observers is based on finding a matrix gain satisfying a certain condition, such as a solution to a matrix inequality. The state estimates are guaranteed to converge to the actual ones if a solution to the LMI exists. In contrast, KF methods do not require that.
- *Unknown Initial Conditions:* Observer designs are independent on the knowledge of the initial conditions of the system. However, if the estimator's initial condition is chosen to be reasonably different from the actual one, estimates from KF might not converge to the actual ones.
- *Robustness to Model Uncertainty and Cyber Attacks:* The observer in Section V and the CKF outperforms UKF (SR-UKF) and EKF in the state estimation under model uncertainty and attack vectors. The observer is robust to model uncertainties because it only assumes that the nonlinearities in the power system dynamics (i.e., $\boldsymbol{\phi}(\mathbf{x})$) satisfy the quadratic inner-boundedness and the one-sided Lipschitz condition. As in Section IV-C, CKF is more robust mostly due to its more accurate cubature approach, which, however, requires more careful investigation. With that in mind, it is hard to generalize. Therefore, advanced theoretical

understanding and more numerical experiments vis-à-vis robustness to model uncertainty and attacks are both needed.

- *Tolerance to Process and Measurement Noise:* The observer in Section V is tolerant to measurement and process noise similar to those assumed for KFs. By design, the KF techniques are developed to deal with such noise assuming statistical distributions are provided. However, many observers do not assume any statistical information regarding unknown inputs.
- *Convergence Guarantees:* Observers have theoretical guarantees for convergence while for the KF techniques there is no strict proof to guarantee that the estimation converges to actual states.
- *Numerical Stability:* Observers do not have numerical stability problems while UKF can encounter numerical instability because the estimation error covariance matrix is not always guaranteed to be positive semi-definite [34].
- *Tolerance to Parametric Inaccuracy:* KF-based methods can tolerate inaccurate parameters to some extent. Dynamic observers deal with parametric uncertainty in the sense that all uncertainties can be augmented to the unknown input component in the state dynamics ($\boldsymbol{B}_{\mathrm{w}}\mathbf{w}$).
- *Computational Complexity:* The CKF, UKF (SR-UKF), and EKF all have computational complexity of $\mathcal{O}(n^3)$ [21], [32]. Since the observers' matrix gains are obtained offline by solving LMIs, observers are easier to implement as only the dynamics are needed in the estimation.

VIII. CONCLUSION AND FUTURE WORK

In this paper, we discuss different DSE methods by presenting an overview of state-of-the-art estimation techniques and developing alternatives, including the CKF and dynamic observers, to address major limitations of existing methods such as intolerance to inaccurate system model and malicious cyber attacks. The proposed methods are extensively tested on a 16-machine 68-bus power system, under significant model uncertainty and cyber attacks against the synchrophaosr measurements. It is shown that the CKF and the observer are more robust to model uncertainty and cyber attacks.

Based on the theoretical capabilities and the experimental results, we summarize the strengths and weaknesses of different estimation techniques especially for power system DSE. We acknowledge that some of these comparisons, such as tolerance to process and measurement noise, are mostly based on numerical results. As future work we will more theoretically investigate and analyze the observer in comparison with Kalman filters, based on which better defending strategies against model uncertainties and cyber attacks against measurements will be developed. Specifically, future work will focus on deriving matrix inequalities that analytically capture robustness in the observer state estimation process with theoretical guarantees. This will be investigated jointly with a nonlinear PMU measurement model, rather than a linearized one.

REFERENCES

[1] A. Monticelli, "Electric power system state estimation," *Proc. IEEE*, vol. 88, no. 2, pp. 262–282, Feb. 2000.
[2] A. Abur and A. G. Expósito, *Power System State Estimation: Theory and Implementation* (Power Engineering (Willis)). Boca Raton, FL, USA: CRC Press, 2004.
[3] J.-J. Qi, G.-Y. He, S.-W. Mei, and Z.-D. Gu, "A review of power system robust state estimation," *Adv. Technol. Elect. Eng. Energy*, vol. 30, no. 3, pp. 59–64, Jul. 2011.
[4] G. He, S. Dong, J. Qi, and Y. Wang, "Robust state estimator based on maximum normal measurement rate," *IEEE Trans. Power Syst.*, vol. 26, no. 4, pp. 2058–2065, Nov. 2011.
[5] J. Qi, G. He, S. Mei, and F. Liu, "Power system set membership state estimation," in *Proc. IEEE Power Energy Soc. Gen. Meeting*, Jul. 2012, pp. 1–7.
[6] K. Zhou, J. C. Doyle, and K. Glover, *Robust and Optimal Control*. Englewood Cliffs, NJ, USA: Prentice-Hall, 1996.
[7] Z. Huang, P. Du, D. Kosterev, and S. Yang, "Generator dynamic model validation and parameter calibration using phasor measurements at the point of connection," *IEEE Trans. Power Syst.*, vol. 28, no. 2, pp. 1939–1949, May 2013.
[8] M. A. M. Ariff, B. C. Pal, and A. K. Singh, "Estimating dynamic model parameters for adaptive protection and control in power system," *IEEE Trans. Power Syst.*, vol. 30, no. 2, pp. 829–839, Mar. 2015.
[9] Y. Liu, P. Ning, and M. K. Reiter, "False data injection attacks against state estimation in electric power grids," *ACM Trans. Inf. Syst. Secur.*, vol. 14, no. 1, pp. 13:1–13:33, Jun. 2011.
[10] O. Kosut, L. Jia, R. J. Thomas, and L. Tong, "Malicious data attacks on the smart grid," *IEEE Trans. Smart Grid*, vol. 2, no. 4, pp. 645–658, Dec. 2011.
[11] O. Vukovic, K. C. Sou, G. Dan, and H. Sandberg, "Network-aware mitigation of data integrity attacks on power system state estimation," *IEEE J. Sel. Areas Commun.*, vol. 30, no. 6, pp. 1108–1118, Jul. 2012.
[12] Q. Yang, J. Yang, W. Yu, D. An, N. Zhang, and W. Zhao, "On false data-injection attacks against power system state estimation: Modeling and countermeasures," *IEEE Trans. Parallel Distrib. Syst.*, vol. 25, no. 3, pp. 717–729, Mar. 2014.
[13] D. Wang, X. Guan, T. Liu, Y. Gu, C. Shen, and Z. Xu, "Extended distributed state estimation: A detection method against tolerable false data injection attacks in smart grids," *Energies*, vol. 7, no. 3, pp. 1517–1538, Mar. 2014.
[14] Q. Yang, D. An, R. Min, W. Yu, X. Yang, and W. Zhao, "On optimal PMU placement-based defense against data integrity attacks in smart grid," *IEEE Trans. Inf. Forensics Security*, vol. 12, no. 7, pp. 1735–1750, Jul. 2017.
[15] Q. Yang, L. Chang, and W. Yu, "On false data injection attacks against Kalman filtering in power system dynamic state estimation," *Secur. Commun. Netw.*, vol. 9, no. 9, pp. 833–849, Jun. 2016.
[16] A. F. Taha, J. Qi, J. Wang, and J. H. Panchal, "Risk mitigation for dynamic state estimation against cyber attacks and unknown inputs," *IEEE Trans. Smart Grid*, vol. 9, no. 2, pp. 886–899, Mar. 2018.
[17] R. E. Kalman, "A new approach to linear filtering and prediction problems," *J. Basic Eng.*, vol. 82, no. 1, pp. 35–45, Mar. 1960.
[18] A. H. Jazwinski, *Stochastic Processes and Filtering Theory*. Chelmsford, MA, USA: Courier Corporation, 2007.
[19] S. J. Julier and J. K. Uhlmann, "New extension of the Kalman filter to nonlinear systems," *Proc. SPIE*, vol. 3068, pp. 182–193, Jul. 1997.
[20] S. J. Julier and J. K. Uhlmann, "Unscented filtering and nonlinear estimation," *Proc. IEEE*, vol. 92, no. 3, pp. 401–422, Mar. 2004.
[21] I. Arasaratnam and S. Haykin, "Cubature Kalman filters," *IEEE Trans. Autom. Control*, vol. 54, no. 6, pp. 1254–1269, Jun. 2009.
[22] W. Kang, A. J. Krener, M. Xiao, and L. Xu, "A survey of observers for nonlinear dynamical systems," in *Data Assimilation for Atmospheric, Oceanic and Hydrologic Applications*, vol. 2. Berlin, Germany: Springer, 2013, pp. 1–25.
[23] A. Radke and Z. Gao, "A survey of state and disturbance observers for practitioners," in *Proc. Amer. Control Conf.*, Jun. 2006, pp. 5183–5188.

[24] Z. Hidayat, R. Babuska, B. De Schutter, and A. Núñez, "Observers for linear distributed-parameter systems: A survey," in *Proc. IEEE Int. Symp. Robot. Sensors Environ. (ROSE)*, Sep. 2011, pp. 166–171.

[25] Z. Huang, K. Schneider, and J. Nieplocha, "Feasibility studies of applying Kalman filter techniques to power system dynamic state estimation," in *Proc. Power Eng. Conf.*, Dec. 2007, pp. 376–382.

[26] E. Ghahremani and I. Kamwa, "Dynamic state estimation in power system by applying the extended Kalman filter with unknown inputs to phasor measurements," *IEEE Trans. Power Syst.*, vol. 26, no. 4, pp. 2556–2566, Nov. 2011.

[27] G. Valverde and V. Terzija, "Unscented Kalman filter for power system dynamic state estimation," *IET Gener., Transmiss. Distrib.*, vol. 5, no. 1, pp. 29–37, Jan. 2011.

[28] E. Ghahremani and I. Kamwa, "Online state estimation of a synchronous generator using unscented Kalman filter from phasor measurements units," *IEEE Trans. Energy Convers.*, vol. 26, no. 4, pp. 1099–1108, Dec. 2011.

[29] S. Wang, W. Gao, and A. P. S. Meliopoulos, "An alternative method for power system dynamic state estimation based on unscented transform," *IEEE Trans. Power Syst.*, vol. 27, no. 2, pp. 942–950, May 2012.

[30] A. K. Singh and B. C. Pal, "Decentralized dynamic state estimation in power systems using unscented transformation," *IEEE Trans. Power Syst.*, vol. 29, no. 2, pp. 794–804, Mar. 2014.

[31] K. Sun, J. Qi, and W. Kang, "Power system observability and dynamic state estimation for stability monitoring using synchrophasor measurements," *Control Eng. Pract.*, vol. 53, pp. 160–172, Aug. 2016.

[32] R. Van der Merwe and E. A. Wan, "The square-root unscented Kalman filter for state and parameter-estimation," in *Proc. IEEE Int. Conf. Acoust., Speech, Signal Process.*, vol. 6, May 2001, pp. 3461–3464.

[33] J. Qi, K. Sun, and W. Kang, "Optimal PMU placement for power system dynamic state estimation by using empirical observability Gramian," *IEEE Trans. Power Syst.*, vol. 30, no. 4, pp. 2041–2054, Jul. 2015.

[34] J. Qi, K. Sun, J. Wang, and H. Liu, "Dynamic state estimation for multi-machine power system by unscented Kalman filter with enhanced numerical stability," *IEEE Trans. Smart Grid*, vol. 9, no. 2, pp. 1184–1196, Mar. 2018.

[35] J. Qi, K. Sun, and W. Kang, "Adaptive optimal PMU placement based on empirical observability Gramian," *IFAC-PapersOnLine*, vol. 49, no. 18, pp. 482–487, Jan. 2016.

[36] N. Zhou, D. Meng, and S. Lu, "Estimation of the dynamic states of synchronous machines using an extended particle filter," *IEEE Trans. Power Syst.*, vol. 28, no. 4, pp. 4152–4161, Nov. 2013.

[37] Y. Cui and R. Kavasseri, "A particle filter for dynamic state estimation in multi-machine systems with detailed models," *IEEE Trans. Power Syst.*, vol. 30, no. 6, pp. 3377–3385, Nov. 2015.

[38] N. Zhou, D. Meng, Z. Huang, and G. Welch, "Dynamic state estimation of a synchronous machine using PMU data: A comparative study," *IEEE Trans. Smart Grid*, vol. 6, no. 1, pp. 450–460, Jan. 2015.

[39] M. A. Gandhi and L. Mili, "Robust Kalman filter based on a generalized maximum-likelihood-type estimator," *IEEE Trans. Signal Process.*, vol. 58, no. 5, pp. 2509–2520, May 2010.

[40] J. Zhang, G. Welch, G. Bishop, and Z. Huang, "A two-stage Kalman filter approach for robust and real-time power system state estimation," *IEEE Trans. Sustain. Energy*, vol. 5, no. 2, pp. 629–636, Apr. 2014.

[41] J. Zhao, M. Netto, and L. Mili, "A robust iterated extended Kalman filter for power system dynamic state estimation," *IEEE Trans. Power Syst.*, vol. 32, no. 4, pp. 3205–3216, Jul. 2017.

[42] J. Zhao, "Dynamic state estimation with model uncertainties using H_∞ extended Kalman filter," *IEEE Trans. Power Syst.*, vol. 33, no. 1, pp. 1099–1100, Jan. 2018.

[43] J. Zhao and L. Mili, "Robust unscented Kalman filter for power system dynamic state estimation with unknown noise statistics," *IEEE Trans. Smart Grid*, to be published.

[44] A. A. Hajnoroozi, F. Aminifar, and H. Ayoubzadeh, "Generating unit model validation and calibration through synchrophasor measurements," *IEEE Trans. Smart Grid*, vol. 6, no. 1, pp. 441–449, Jan. 2015.

[45] J. Chen and R. J. Patton, *Robust Model-Based Fault Diagnosis for Dynamic Systems*. Springer Science & Business Media, 2012.

[46] A. M. Pertew, H. J. Marquez, and Q. Zhao, "Design of unknown input observers for Lipschitz nonlinear systems," in *Proc. Amer. Control Conf.*, Jun. 2005, pp. 4198–4203.

[47] A. Lee, "Electric sector failure scenarios and impact analyses," Electr. Power Res. Inst., Palo Alto, CA, USA, Tech. Rep., Sep. 2013.

[48] S. Sridhar, A. Hahn, and M. Govindarasu, "Cyber–physical system security for the electric power grid," *Proc. IEEE*, vol. 100, no. 1, pp. 210–224, Jan. 2012.

[49] J. Lu and R. Niu, "False information injection attack on dynamic state estimation in multi-sensor systems," in *Proc. 17th Int. Conf. Inf. Fusion (FUSION)*, Jul. 2014, pp. 1–8.

[50] S. Wang, J. Zhao, Z. Huang, and R. Diao, "Assessing Gaussian assumption of PMU measurement error using field data," *IEEE Trans. Power Del.*, to be published.

[51] J. K. Uhlmann, "Simultaneous map building and localization for real time applications," Transfer thesis, Univ. Oxford, Oxford, U.K., 1994.

[52] R. Bellman and R. Bellman, *Adaptive Control Processes: A Guided Tour* (Rand Corporation. Research Studies). Princeton, NJ, USA: Princeton Univ. Press, 1961.

[53] S. A. Gadsden, M. Al-Shabi, I. Arasaratnam, and S. R. Habibi, "Combined cubature Kalman and smooth variable structure filtering: A robust nonlinear estimation strategy," *Signal Process.*, vol. 96, pp. 290–299, Mar. 2014.

[54] W. Zhang, H. Su, H. Wang, and Z. Han, "Full-order and reduced-order observers for one-sided Lipschitz nonlinear systems using Riccati equations," *Commun. Nonlinear Sci. Numer. Simul.*, vol. 17, no. 12, pp. 4968–4977, Dec. 2012.

[55] D. D. Siljak, D. M. Stipanovic, and A. I. Zecevic, "Robust decentralized turbine/governor control using linear matrix inequalities," *IEEE Trans. Power Syst.*, vol. 17, no. 3, pp. 715–722, Aug. 2002.

[56] J. Qi, J. Wang, H. Liu, and A. D. Dimitrovski, "Nonlinear model reduction in power systems by balancing of empirical controllability and observability covariances," *IEEE Trans. Power Syst.*, vol. 32, no. 1, pp. 114–126, Jan. 2017.

[57] M. Vidyasagar, *Nonlinear Systems Analysis*. Philadelphia, PA, USA: SIAM, 2002.

[58] S. Boyd, L. El Ghaoui, E. Feron, and V. Balakrishnan, *Linear Matrix Inequalities in System and Control Theory*, vol. 15. SIAM, 1994.

[59] J. H. Chow and K. W. Cheung, "A toolbox for power system dynamics and control engineering education and research," *IEEE Trans. Power Syst.*, vol. 7, no. 4, pp. 1559–1564, Nov. 1992.

[60] S. Julier, J. Uhlmann, and H. F. Durrant-Whyte, "A new method for the nonlinear transformation of means and covariances in filters and estimators," *IEEE Trans. Autom. Control*, vol. 45, no. 3, pp. 477–482, Mar. 2000.

[61] J. Hartikainen, A. Solin, and S. Särkkä, "Optimal filtering with Kalman filters and smoothers," Dept. Biomed. Eng. Comput. Sci., Aalto Univ. School Sci., Espoo, Finland, Tech. Rep., Aug. 2011.

[62] M. Grant, S. Boyd, and Y. Ye, "CVX: MATLAB software for disciplined convex programming," Tech. Rep., 2008.

JUNJIAN QI (S'12–M'13–SM'17) received the B.E. degree in electrical engineering from Shandong University, Jinan, China, in 2008, and the Ph.D. degree in electrical engineering from Tsinghua University, Beijing, China, in 2013. He was a Visiting Scholar with Iowa State University, Ames, IA, USA, in 2012, a Research Associate with the Department of EECS, University of Tennessee, Knoxville, TN, USA, from 2013 to 2015, and a Post-Doctoral Appointee with the Energy Systems Division, Argonne National Laboratory, Argonne, IL, USA, from 2015 to 2017. He is currently an Assistant Professor with the Department of Electrical and Computer Engineering, University of Central Florida, Orlando, FL, USA.

His research interests include cascading blackouts, power system dynamics, state estimation, synchrophasors, voltage control, and cybersecurity. He is the Secretary of the IEEE Working Group on Energy Internet and the IEEE Task Force on Voltage Control for Smart Grids. He is an Associate Editor of the IEEE Access.

AHMAD F. TAHA received the B.E. and Ph.D. degrees in Electrical and Computer Engineering from the American University of Beirut, Lebanon in 2011 and Purdue University, West Lafayette, Indiana in 2015. He is currently an Assistant Professor with the Department of Electrical and Computer Engineering, The University of Texas at San Antonio, San Antonio. He is interested in understanding how complex cyber-physical systems (CPS) operate, behave, and misbehave. His research focus includes optimization, control, and security of CPSs with applications to power, water, and transportation networks.

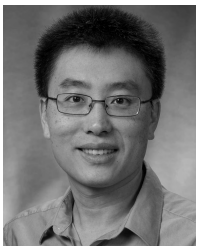

JIANHUI WANG (S'07–SM'12) received the Ph.D. degree in electrical engineering from the Illinois Institute of Technology, Chicago, IL, USA, in 2007. He is currently an Associate Professor with the Department of Electrical Engineering, Southern Methodist University, Dallas, TX, USA.

He has held visiting positions in Europe, Australia, and Hong Kong, including a VELUX Visiting Professorship with the Technical University of Denmark. He is the secretary of the IEEE Power and Energy Society (PES) Power System Operations, Planning and Economics Committee. He is an Associate Editor of the *Journal of Energy Engineering* and an Editorial Board Member of *Applied Energy*.He is the Editor-in-Chief of the IEEE TRANSACTIONS ON SMART GRID and an IEEE PES Distinguished Lecturer. He is also the recipient of the IEEE PES Power System Operation Committee Prize Paper Award in 2015.